FAULT DETECTION USING DIP-STEERED MULTI-TRACE SIMILARITY EXTRACTION TECHNIQUES: CASE STUDY USING OFFSHORE NIGER DELTA 3D SEISMIC DATA

BABANGIDA JIBRIN[1] and WASIU RAJI[2]

[1] *School of Geography, Earth and Environmental Sciences, University of Birmingham, West Midlands B15 2TT, U.K. bjibrin@gmail.com*
[2] *Department of Geophysics, Stanford University, Mitchell Building, Stanford, California, 94305-2215, U.S.A.*

(Received July 16, 2013; revised version accepted December 14, 2013)

ABSTRACT

Jibrin, B. and Raji, W., 2014. Fault detection using dip-steered multi-trace similarity extraction techniques: Case study using offshore Niger Delta 3D seismic data. *Journal of Seismic Exploration, 23: 19-30.*

Techniques for detecting faults have been applied to a 3D seismic data acquired in the shallow offshore Niger Delta. A volume containing the dip and azimuth of the traces was first computed directly from the data. The data was enhanced by applying filters to compute two structurally-improved volumes containing localized and sub-regional seismic dips respectively. Multi-trace similarity was then computed using the seismic reflection and sub-regional dip data as input. The data highlighted discrete zones of dip and similarity anomalies representing listric normal and counter regional faults with improved visibility of wall-rock volumes. The case study demonstrates the potential benefits of applying dip-steering techniques for the enhanced detection of faults and improved visibility of wall-rock volumes next to the faults.

KEY WORDS: Niger Delta, 3D seismic data, dip-steering, steering volumes, multi-trace similarity, fault detection.

INTRODUCTION

A major problem with tracking faults using seismic reflection data is its limited ability to resolve structural features and the difficulty in distinguishing between anomalies related to real geological features and those related to noise. Such uncertainties usually result in time consuming seismic interpretation workflows that could impact on the reliability of subsurface structural models.

0963-0651/14/$5.00

The introduction of the "coherence cube" (Bahorich and Farmer, 1995) has had a major impact as an invaluable tool for highlighting structural and stratigraphic features in seismic data.

Similar algorithms for improving the quality of seismic data have been previously described (Marfurt et al., 1999; Al-Dossary and Marfurt, 2006; Hennings et al., 2010; Chopra and Marfurt, 2011; Qayyum and de Groot, 2012). Faults are important in oil and gas exploration and production, and as the need to discover new reserves in complex structural settings is intensified, the improved resolution of modern 3D seismic data combined with advanced techniques for computing attributes that highlight structural features can play a key role in the accurate detection of faults with improved imaging of fault zone structure.

In this article, we describe a workflow for computing an attribute that measures the volumetric similarity of seismic traces using a 3D seismic volume acquired from the shallow offshore Niger Delta (Fig. 1). Perspective volume and time-slice views of the structurally-enhanced data are used to demonstrate that applying the techniques to the data has improved the quality of fault imaging and the visibility of wall-rock structure next to the faults.

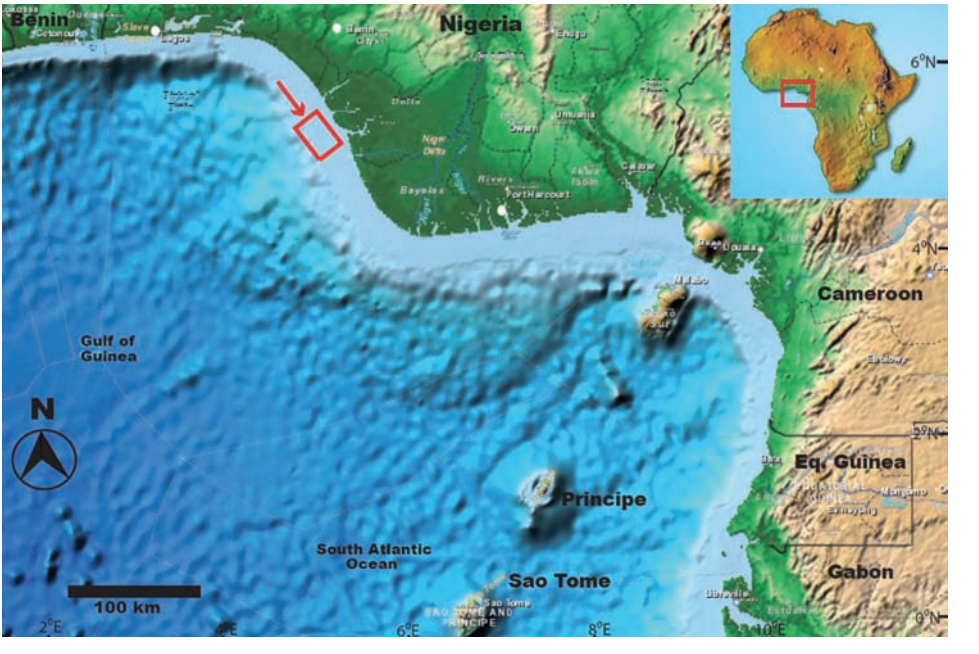

Fig. 1. Map of the Gulf of Guinea showing the location of the study area (red arrow).

METHODS

Data

The 657 km² post stack time-migrated 3D seismic reflection data have inline and crossline spacing of 12.5 m respectively, a recording length of 4 s with a 4 ms sampling. Spectral analysis shows that the dominant frequency in the data varies with depth and ranges from 40 to 60 Hz in the interval where most of the faults are located (0.5 to 3.0 s two-way travel time). A frequency of 46 Hz that appears to be the strongest in the amplitude spectrum plot was used to calculate the resolution of the data. The vertical resolution varies from ~10 m at shallower sections but deteriorates to ~18 m at deeper sections of the data, while the horizontal resolution is < 100 m. The data have a vertical scale in seconds (s) two-way travel time (TWTT).

Workflow

Fig. 2 is a summary of the workflow applied to the data to detect and highlight faults and fault zones.

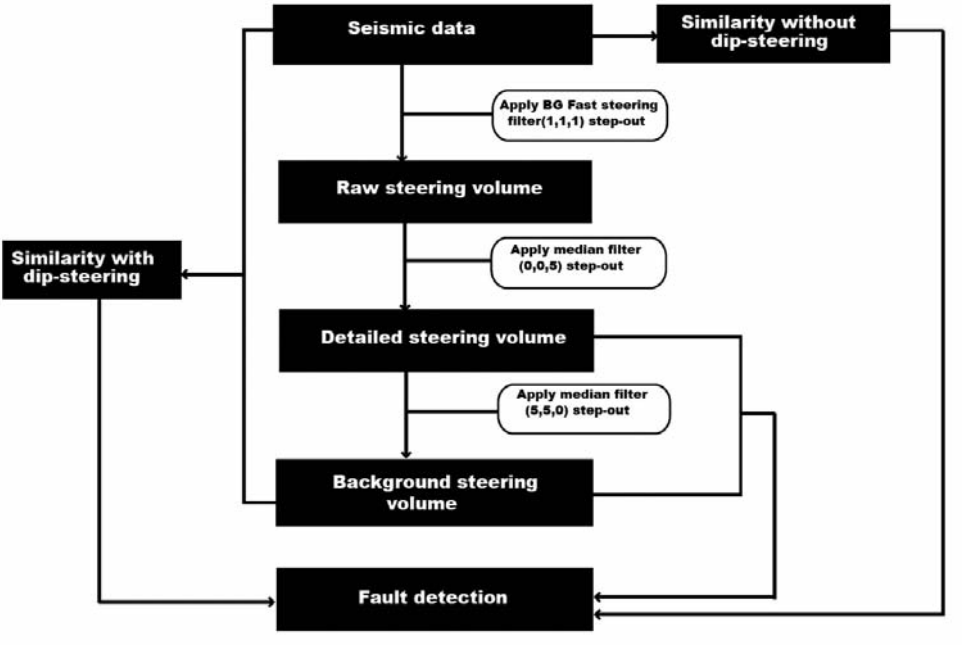

Fig. 2. Workflow for multi-trace dip and similarity computation techniques applied to the data.

Step 1: Multi-trace dip-steering computation

In multi-trace dip-steering computation, attributes are conceptually guided along a 3D surface on which the seismic phase is approximately the same thus creating a virtual horizon at each trace position following the dip/azimuth of the seismic traces from one trace to another. The trace segments are aligned horizontally without the application of dip-steering (Fig. 3a). However, with the application of full steering, the dip and azimuth of the traces is updated at every trace location (Fig. 3b). Thus, the steering data is a volumetric grid of the dip of the seismic traces.

The first steering data was calculated directly from the seismic reflection data using a fast steering filter algorithm based on the analysis of the vertical and horizontal gradient of the amplitude data (Tingdahl, 2003). A step-out of 1,1,1, (i.e., 3 samples) one each in the inline, crossline and time directions was used for the computation, with a filtering distance of 37.5 m in the inline and crossline directions (bin spacing of 12.5 x number of samples) and 12 ms in the time direction (sampling rate of 4 ms x number of samples). This steering data is referred to as the "raw steering" volume.

The second steering data was computed by applying edge preserving median filters to the raw steering volume to attenuate localized noise along structural dips in the vertical (time) direction using a step-out of 0,0,5 (i.e., 5 samples) in the time direction only, with a filtering distance of 20 ms (sampling rate of 4 ms x number of samples). This steering data contain localized dip of the traces and referred to as the "detailed steering" volume.

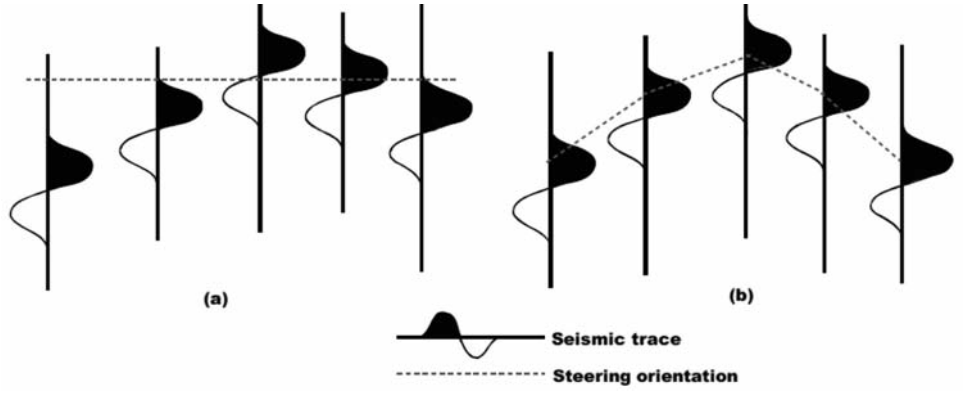

Fig. 3. Cross sectional schematic illustration of dip-steering techniques applied to the data. In Fig. 3a, no steering is applied for multi-trace attribute computation, while in Fig. 3b full dip-steering is applied.

The third steering data was computed by applying edge preserving smoothing filter to the detailed steering volume to smoothen localized noise using a step-out of 5,5,0 (lateral direction). The step-out implies that the filtering is along every 5 inline and 5 crossline traces only (i.e., 10 samples and none in the time direction) with a filtering distance of 125 m in the inline and crossline directions (i.e., bin spacing of 12.5 x number of samples). This data is referred to as the "background steering" volume.

All the steering data were computed on-the-fly and analysed using parameter settings summarized in Table 1 prior to volume processing. Detailed description of the mathematics of dip and azimuth processing applied to the data is described in Tingdahl (2003), Tingdahl and de Groot (2003).

Table 1. Multi-trace dip extraction parameter setting applied to the data.

Input data	Calculation step-out	Filter step-out	No. of samples	Filter type	Output data
Seismic reflection	(1,1,1)	(1,1,1)	1 each in the inline, crossline and time directions	Median	Raw steering
Raw steering		(0,0,5)	5 in the time (vertical) direction only	Median	Detailed steering
Detailed steering		(5,5,0)	5 in the inline and cross line (lateral) directions only	Median	Background steering

Step 2: Multi-trace similarity computation

An attribute that detects and highlights the waveform similarity of adjacent trace pairs and the time difference between the traces interpreted as vectors was computed to highlight faults in the data. Similarity (S) is mathematically the Euclidean distance in hyperspace between vectors of the segments, normalized between 0 and 1 to the sum of the lengths of the vectors [eq. (1)]. A high similarity means the trace segments are similar in wave-shape and amplitude. Low similarity implies that the traces are dissimilar probably due to faulting (Tingdahl, 2003).

$$S = 1 - |v - u|/[|v| + |u|] \ ,$$

i.e., $|\text{trace segment 1} - \text{trace segment 2}|/|\text{trace segment 1} + \text{trace segment 2}|$, (1)

where

$$v = \begin{bmatrix} f(t_1, x_v, y_v) \\ f(t_1+d_t, x_v, y_v) \\ . \\ . \\ f(t_2-d_t, x_v, y_v) \\ f(t_2, x_v, y_v) \end{bmatrix}, \quad u = \begin{bmatrix} f(t_1, x_u, y_u) \\ f(t_1+d_t, x_u, y_u) \\ . \\ . \\ f(t_2-d_t, x_u, y_u) \\ f(t_2, x_u, y_u) \end{bmatrix}.$$

t is the time-depth of investigation, dt is the sampling interval, t_1 and t_2 are the limits of the time gate, (x_v, y_v) and (x_u, y_u) are the two trace positions that are compared, while f is the amplitude value.

Step 3: Applying dip-steering for multi-trace similarity computation

Similarity is sensitive to amplitude differences between trace segments in addition to wave-shape [eq. (1)]. The difference in the response of the attribute at the location of faults is largely dependent on the dip of the traces. By applying the steering algorithm, similarity computation is along trace-to-trace guided by the local dip and azimuth at every position along the track. For fault detection, the application of dip-steering reduces the sensitivity of similarity to dipping reflectors with no apparent link to faulting by aligning adjacent trace segments with a lag time using the concept of dip-steering. The result is that background noise is attenuated while faults are highlighted due to the dissimilarity of the traces.

The input data for similarity computation are the seismic reflection and background steering volumes. Previous work has shown that similarity computed along sub-regional dip (background steering data) provides the best measure of multi-trace similarity (Brouwer and Huck, 2012). For this study, a time gate of +24 ms and −24 ms, equivalent to the average seismic wavelength within the window of investigation and a step-out of 1,1 (i.e., 2 samples) one each in the inline and crossline directions only were used in computing multi-trace similarity. This implies that the attribute computation distance in both the inline and crossline directions is 25 m respectively (bin spacing of 12.5 x number of samples). No sample in the time direction was used for the computation because similarity measures made along time slices (rather than along structural dip) generate artifacts that actually do show geologic features of interest.

All trace pairs defined by the inline, crossline and time position step-out were calculated using the full-block extension, with the position of the minimum similarity selected as the output statistical operator so that dissimilarity values close to 0 are emphasized (i.e., the values of similarity being between 0 and 1, the minimum output statistical operator will show dissimilarity values close to 0 at the location of faults).

Table 2 is a summary of the parameter setting used in computing the attribute. Comprehensive description of the mathematics of similarity calculation is described in Tingdahl (2003), Tingdahl and de Groot (2003), Tingdahl and de Rooij (2005).

Table 2. Multi-trace similarity extraction parameter setting applied to the data.

Input data	**Time gate (ms)**	**Extension**	**Trace step-out**	**No. of samples**	**Dip-steering**	**Statistical output operator**	**Output data**
Seismic reflection	(-24,24)	Full block	(1,1)	1 each in the inline and crossline directions only	None	Minimum	Similarity without dip-steering
Seismic reflection + background steering	(-24,24)	Full block	(1,1)	1 each in the inline and crossline directions only	Full steering	Minimum	Similarity with dip-steering

RESULTS

Fig. 4 show block volumes of the seismic reflectivity and computed dip-steering data spanning 0.5 to 3.0 s two-way travel time with chair-cut display of time-slices extracted at 1.5 s two-way travel time from the data volumes. The red block arrows highlight discrete zones of curvi-linear dip anomalies radiating from the north-western part of the data (blue circles) clearly resolved in the detailed and background steering data (Fig. 4c and Fig. 4d). The green arrows show a NW-SE trending zone of linear dip anomalies. For comparison, these anomalies correlate with narrow zones of low reflectivity in Fig. 4a. Comparing chair-cut volume display of time-slices extracted at 1.5 s two-way travel time from seismic reflection and similarity computed directly from the seismic data, the close correlation between discrete dip and low

similarity anomalies becomes apparently clear (red block arrows in Fig. 4d and Fig. 4e). In addition, the imaging of the NE-SW trending faults in the north-eastern parts of the survey area has been improved (green arrows).

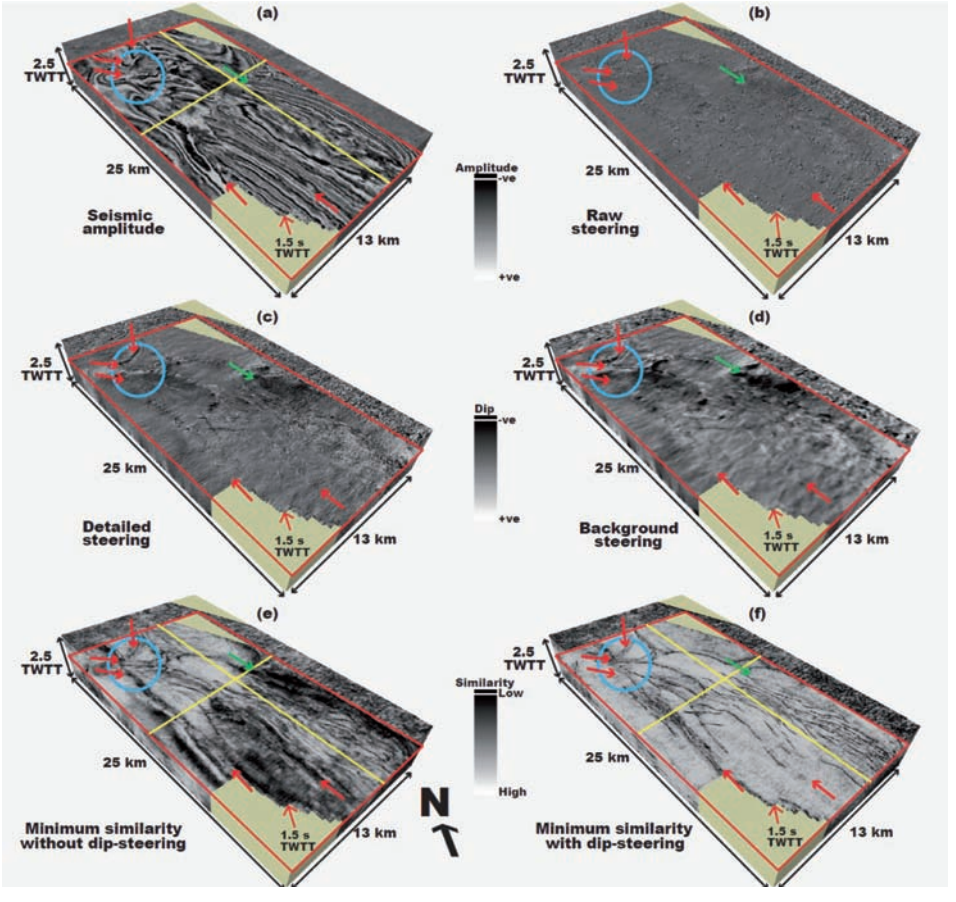

Fig. 4. Perspective volume views of seismic amplitude (a), raw steering (b), detailed steering (c), background steering (d), similarity computed without dip-steering (e), and similarity computed with dip-steering (f). All volumes span 0.5 to 3.0 s two-way travel time. The red outline shows time-slices extracted at 1.5 s two-way travel time, while the yellow lines represent inline and crossline sections shown in Fig. 5 and Fig. 6, respectively.

Comparing chair-cut display of time-slices extracted at 1.5 s two-way travel time from similarity data computed without the application of dip steering (Fig. 4e) with similarity computed along sub-regional dips (Fig. 4f), the effect of applying dip-steering becomes evident. Although discontinuities have been detected in the two data volumes, the imaging and contrast of the faults have been significantly improved with dip-steering, while the contrast at the location of the faults is poor with a noisier background in similarity computed directly from the seismic reflection data (without dip-steering).

In vertical cross sections, faults are located at zones of vertically displaced reflectors with a normal sense of direction (red arrows in Fig. 5a and Fig. 6a). In the similarity cross sections, faults are located at clearly defined linear/listric discrete zones of low similarity. However, comparing similarity calculated with and without the application of dip-steering, the edges of the faults is sharper with significantly improved contrast in the former (Fig. 5c and Fig. 6c). Furthermore, the contrast of the synthetic and antithetic faults that deform the large-scale anticline has been improved with the application of dip-steering (Fig. 5c). In addition, the contrast and visibility of wall-rock volumes next to the listric faults has also been enhanced. In Fig. 5b and Fig. 6b, the dipping reflectors next to the faults exhibit anomalously low similarity and poor contrast (yellow arrows). However, the application of dip-steering for similarity computation has improved the contrast and visibility of fault zones by correcting for the anomalous similarity due to dipping reflectors (yellow arrows in Fig. 5c and Fig. 6c).

CONCLUSION

A workflow has been described for improving the quality of fault imaging in a 3D Niger Delta seismic data using dip-steering and multi-trace similarity computation techniques. The structurally-enhanced data detected discrete zones of dip and similarity anomalies representing the location of basinward-dipping normal and counter regional faults. Perspective volume and cross sectional views of the data show that the imaging of the faults and visibility of wall-rock volumes have been improved by the application of dip-steering in comparison to similarity computed directly from the seismic data. The enhanced imaging of the discontinuities can improve the quality of seismic interpretation so that traces of the faults are tracked with a good degree of certainty. The improved visibility of the wall-rock volumes can guide detailed interpretation of fault zone structure at the scale of seismic resolution.

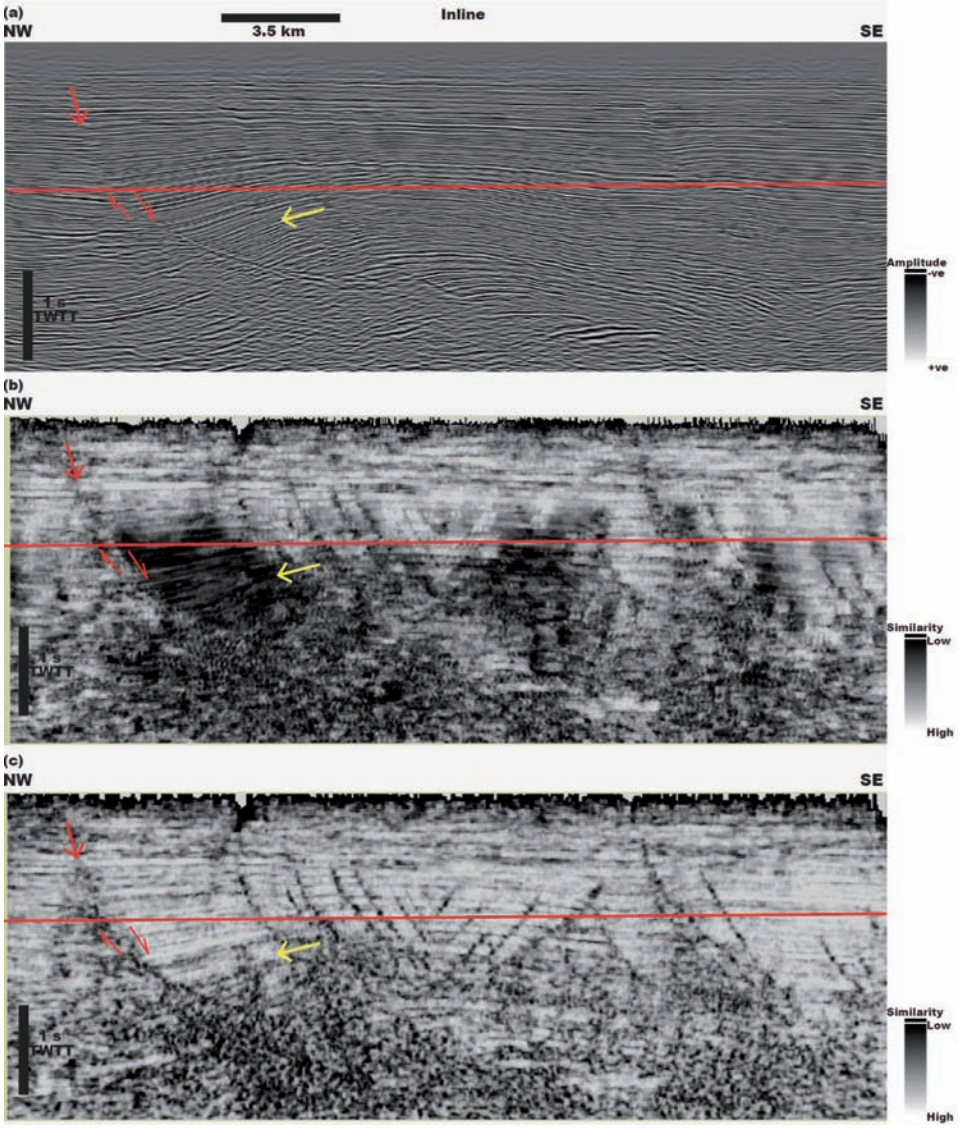

Fig. 5. Inline cross sectional views of seismic reflection (a), similarity computed without dip-steering (b), and similarity computed with dip-steering (c). The red line is the location of time-slices extracted at 1.5 s two-way travel time. Vertical scale is in seconds (two-way travel time) and horizontal scale is in kilometres. Vertical exaggeration is ~3 x the horizontal scale.

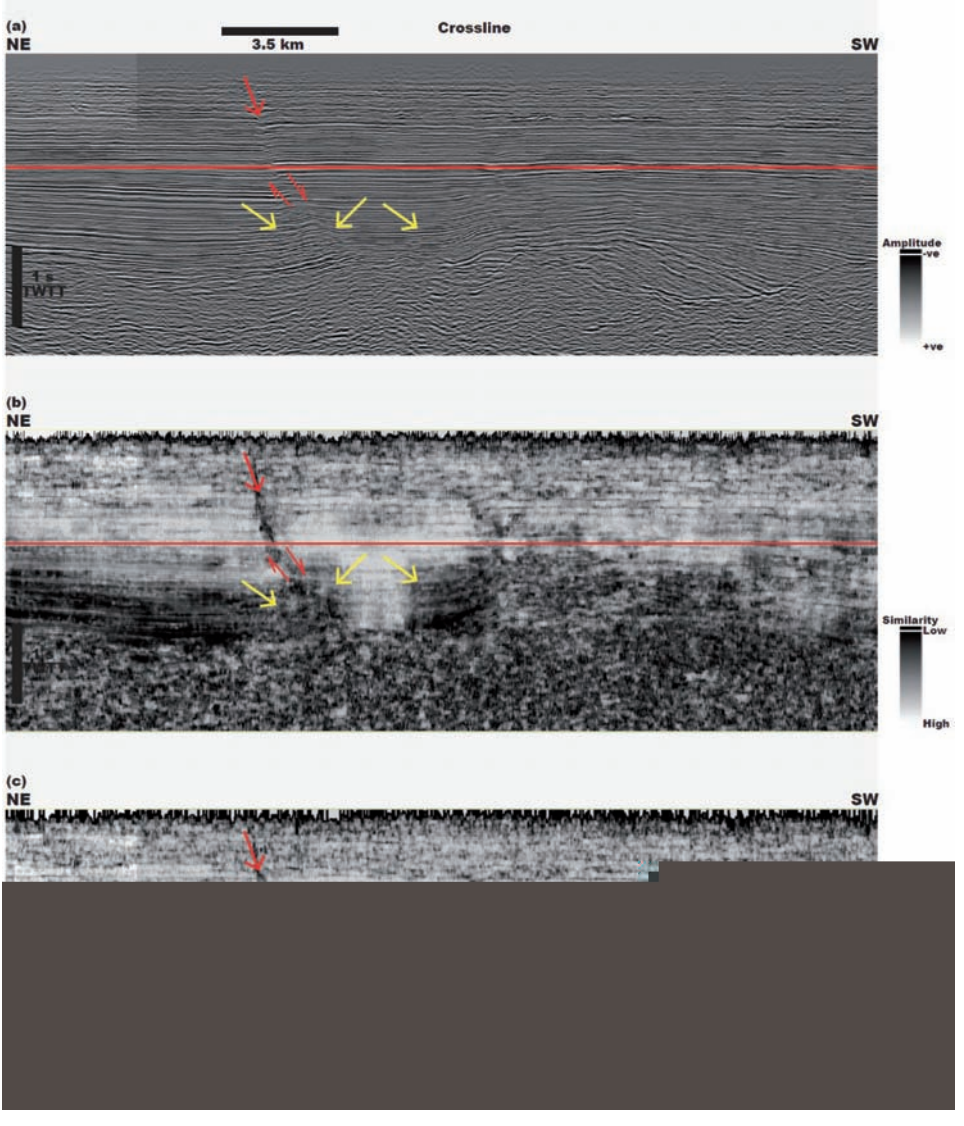

Fig. 6. Vertical crossline views of seismic reflection (a), similarity computed without dip-steering (b), and similarity computed with dip-steering (c). The red line is the location of time-slices extracted at 1.5 s two-way travel time. Vertical scale is in seconds (two-way travel time) and horizontal scale is in kilometres. Vertical exaggeration is ~3 x the horizontal scale.

ACKNOWLEDGEMENTS

The authors are grateful to the company that provided the data and dGB Earth Sciences for donating OpendTect software for academic use at the University of Birmingham. Saleh Al-Dossary (Saudi-Aramco) and Eric Bounga (dGB Earth Sciences) are thanked for reviewing drafts of the manuscript and for providing useful suggestions that improved the quality of the article.

REFERENCES

Al-Dossary, S. and Marfurt, K.J., 2006. 3D volumetric multi-spectral estimates of reflector curvature and rotation. Geophysics, 17 (5): 41-45.

Bahorich, M.S. and Farmer, S.L., 1995. 3-D seismic coherency for faults and stratigraphic features. The Leading Edge, 14: 1053-1058.

Brouwer, F. and Huck, A., 2012. An integrated workflow to optimize discontinuity attributes for imaging of faults. Attributes: New views on seismic imaging - Their use in exploration and production. Abstr., 1st GCSSEPM Conf., 21: 496-533.

Chopra, S. and Marfurt, K.J., 2011. Coherence and curvature attributes on preconditioned seismic data. The Leading Edge, 30: 386-393.

Hennings, A.T., Martin, R. and Paton, G., 2010. Data conditioning and seismic attribute analysis in the Eagle Ford Shale Play: Examples from Sinor Ranch, Live Oak County. Expanded Abstr., 80th Ann. Internat. SEG Mtg., Denver.

Marfurt, K.J., Sudakher, V., Gersztenkorn, A., Crawford, K.D. and Nissen, S.E., 1999. Coherency calculations in the presence of structural dip. Geophysics, 64: 104-111.

Qayyum, F., and de Groot, P., 2012. Seismic dips help unlock reservoirs. Am. Oil Gas Rep.: 75-79.

Tingdahl, K.M., 2003. Improving seismic chimney detection using directional attributes. Develop. Petrol. Sci., 51: 157-173.

Tingdahl, K. and de Groot, P., 2003. Post-stack dip and azimuth processing. J. Seismic Explor., 12: 113-126.

Tingdahl, K.M. and de Rooij, M., 2005. Semi-automatic detection of faults in 3-D seismic data. Geophys. Prosp., 53: 533-542.